Official journal of the CIOMP 2047-7538
www.nature.com/lsa

ARTICLE Open Access

Color coded metadevices toward programmed terahertz switching

Weibao He[1,2,3], Xiang'ai Cheng[1,2,3], Siyang Hu[1], Ziheng Ren[1], Zhongyi Yu[1], Shun Wan[1], Yuze Hu[4]✉ and Tian Jiang[4]✉

Abstract

Terahertz modulators play a critical role in high-speed wireless communication, non-destructive imaging, and so on, which have attracted a large amount of research interest. Nevertheless, all-optical terahertz modulation, an ultrafast dynamical control approach, remains to be limited in terms of encoding and multifunction. Here we experimentally demonstrated an optical-programmed terahertz switching realized by combining optical metasurfaces with the terahertz metasurface, resulting in 2-bit dual-channel terahertz encoding. The terahertz metasurface, made up of semiconductor islands and artificial microstructures, enables effective all-optical programming by providing multiple frequency channels with ultrafast modulation at the nanosecond level. Meanwhile, optical metasurfaces covered in terahertz metasurface alter the spatial light field distribution to obtain color code. According to the time-domain coupled mode theory analysis, the energy dissipation modes in terahertz metasurface can be independently controlled by color excitation, which explains the principle of 2-bit encoding well. This work establishes a platform for all-optical programmed terahertz metadevices and may further advance the application of composite metasurface in terahertz manipulation.

Introduction

Miniaturization and higher integration of on-chip optical systems[1] necessitate more device adaptability, versatility, and data storage capacity[2–5]. Metasurfaces, a form of ultrathin planar optical component, have emerged as an advanced scheme for controlling light and enabling a wide range of optical applications in previous studies[6–12]. Especially for terahertz waves with high-capacity communications, metasurfaces provide a potential solution to the lack of functional devices. Terahertz metasurfaces have addressed a great number of scientific and technological challenges, delivering essential assistance for boosting the development of terahertz functional devices[13–19]. Scalable metasurfaces with individually programmable elements, simultaneous amplitude and phase control, and gigahertz-speed reconfiguration are required to fulfill the full promise of reconfigurable features and enable sophisticated electromagnetic transformations. Reconfigurability in active terahertz metasurfaces has been demonstrated with liquid crystal[20–22], phase-change materials[23–25], mechanical systems[26,27], and two-dimensional materials[28,29]. These approaches, however, usually have a poor response time, are not scalable, and require substantial external stimuli. To increase the capacity of information transmission, ultrafast terahertz switching and programmability will need to be combined for the next generation of integrated devices.

Light-driven reconfigurable metasurfaces that carry modulation information in amplitude, phase, frequency, and polarization are receiving a great deal of attention and research due to their contactless, succinct construction and ultrafast response-ability[30–38]. The ultrafast modulation behavior benefits significantly from the photogenerated carrier relaxation dynamics of active materials, in particular intrinsic epitaxial silicon (Si) and amorphous germanium, which have lower preparation costs with relaxation times in the order of nanoseconds and picoseconds[39–42]. These materials are advantageous in the preparation of ultrafast terahertz metadevices. In general, the limitation of materials leads to the single function of optically controlled terahertz devices, yet we have recently conducted some exploratory works on multi-functional and multi-dimensional all-optical terahertz metasurfaces[43–45]. Nevertheless, as opposed to

Correspondence: Yuze Hu (hyz_yj@sina.com) or
Tian Jiang (tjiang@nudt.edu.cn)
[1]College of Advanced Interdisciplinary Studies, National University of Defense Technology, Changsha, China
[2]Nanhu Laser Laboratory, National University of Defense Technology, Changsha, China
Full list of author information is available at the end of the article

© The Author(s) 2024
Open Access This article is licensed under a Creative Commons Attribution 4.0 International License, which permits use, sharing, adaptation, distribution and reproduction in any medium or format, as long as you give appropriate credit to the original author(s) and the source, provide a link to the Creative Commons licence, and indicate if changes were made. The images or other third party material in this article are included in the article's Creative Commons licence, unless indicated otherwise in a credit line to the material. If material is not included in the article's Creative Commons licence and your intended use is not permitted by statutory regulation or exceeds the permitted use, you will need to obtain permission directly from the copyright holder. To view a copy of this licence, visit http://creativecommons.org/licenses/by/4.0/.

electronic-coding terahertz modulation which is more concerned, optical coding processes have received comparatively little research. Though some efforts excite high-resistance silicon wafers for terahertz imaging using spatial light modulators as encoding masks[46–50], they mostly focus on single-channel modulation and suffer from low coding speed. Further research is highly required on integrated and miniaturized light-coded metadevices toward programmed ultrafast terahertz switching.

In this work, we have prepared an optically controlled terahertz 2-bit encoding device by combing photonic crystals, i.e., arranged Distributed Bragg Reflector (DBR) microstrips, with terahertz metal metasurface. In terahertz metasurfaces, the multimode coupling effect is intended to provide extreme sensitivity, multi-channel resonances, and enhanced modulation efficiency. Intrinsic epitaxial silicon islands are embedded in split resonant resonators (SRRs) of metal metasurface to control its non-radiative loss for ultrafast modulation behavior. The DBR microstrips that block light at 400 nm and 800 nm tightly integrate with the terahertz metasurface structure and are positioned on the metal metasurface units, resulting in different couple mode dissipations controlled by pump-color excitation. We experimentally tested the 2-bit optical terahertz programming behavior on this integrated metadevice. Mutual verification was conducted through experiments and numerical simulations. In addition, the time-domain coupled mode theory (TCMT) has been proposed to explain the physical mechanism, revealing that the free-standing non-radiative losses of the coupling modes are the foundation of dual channel coding. This optical-programming terahertz-switching method, which has yet to be proposed, is experimentally demonstrated in our metadevice that combines optical metasurface and terahertz metasurface. Our work provides a new paradigm for optically controlled terahertz encoding.

Results

Design of color-coded metadevice

Multidimensional electromagnetic responses exist in open multimode systems and the challenge of their independent controlling resides in actively tailoring terahertz waves, that is, simple coupling modes, that maximize their functionality. A sketch of a color-coded metadevice is shown in Fig. 1. Our system consists of a bilayer structure made of coupling terahertz resonators with detuned modes and Distributed Bragg Reflector (DBR) microstrips with two-color spectral filtering. Of interest here is the combination between optical metasurface with dielectric photonic crystal and active terahertz metasurface, which can implement optical encoding terahertz modulation, as shown in Fig. 1b. For the terahertz metasurface, it is vital to realize various resonant features at subwavelength scale, whose lineshapes should be sensitive to the external perturbation. Here, the double electromagnetically induced transparency (EIT) effect with a bright dipole moment coupled with four dark inductive-capacitive resonances is selected to meet these prerequisites. The mode detuning is implemented by breaking the mirror symmetry of a typical EIT meta-system using SRRs of distinct sizes (Fig. 1d), leading to three hybrid modes. Its radiative lineshape is experimentally measured in Fig. 1g. When a 200-nm-thick semiconductor epitaxial layer (silicon, bandgap ~1.1 eV) is incorporated in the SRRs, the terahertz responses can be actively controlled by an external optical excitation. We choose Si as the active material in this case instead of other materials like TMDCs[51,52], amorphous germanium[40], perovskite[31], etc., which are used for all-optical controlled terahertz modulation, for two reasons: (i) The periodic active islands incorporated in SRRs can be fabricated with mature techniques. (ii) More photogenerated carriers of Si can be produced with the same pump fluence, leading to a higher modulation efficiency compared to other semiconductor film materials. For color-coded metadevice, the DBR microstrips with quasi-infinite in the x-y plane and periodic out of the plane are introduced to filter out different pump colors. Here, two DBR microstrips that consist of multiple iterations of Nb_2O_5 and SiO_2 with optimized optical thickness (Table S1 and S2 in the Supporting Information) are built to cover SRRs on both sides of the cut-wire compactly (Fig. 1c). As we can see from the Fig. 1e and Fig. 1f, in experiment the DBR_1 reflects pump light of 800 nm and transmits that of 400 nm, while the DBR_2 is exactly the opposite. Upon this, the non-radiative damping rate of each type of coupling metaatom (CM_1 and CM_2) can be controlled independently by applying different pumping colors to achieve the encoding of terahertz amplitudes. Our fantastic innovation is the combination of terahertz metasurface with arranged optical-band DBRs. Without DBRs, color coding is not possible, and both terahertz channels will be modulated concurrently with whichever pumping wavelengths. The specific size parameters of the metal metasurface structure are described in detail in the Supporting Information (Fig. S1), and the metadevice processing process can be found in the Methods section.

Performance of pumping color-coded functionality

A multimode system based on the proposed EIT metasurface provides channels for multidimensional information manipulation. To demonstrate the encoding behavior, experimentally extracted magnitude changes at two channels with different excitation wavelengths are described in Fig. 2. Three basic modulation methods can be easily implemented: (i) When the metadevice pumped by λ_1 (400 nm), the non-radiative damping of CM_1 increases and then the EIT resonance of the left channel is suppressed (Fig. 2a). (ii) When the metadevice pumped by λ_2 (800 nm), the loss of CM_2 increases and the right channel is quenched (Fig. 2b). (iii) When the metadevice

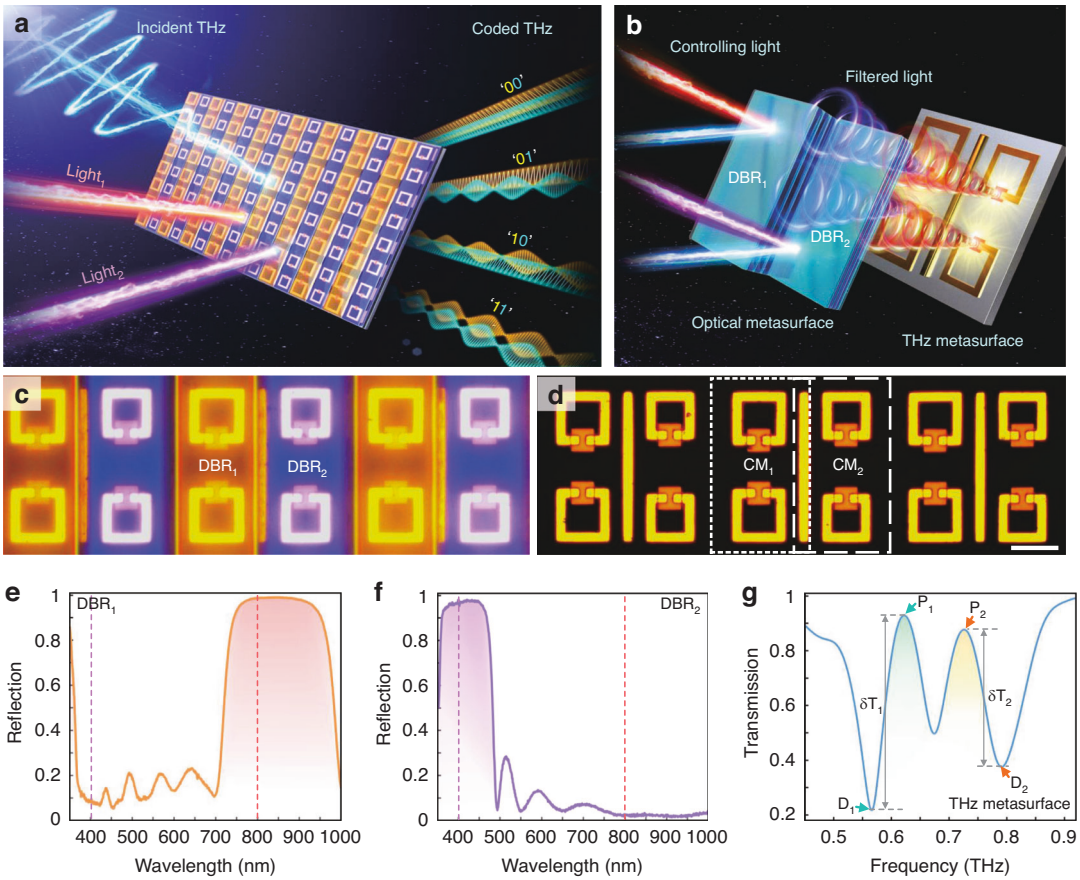

Fig. 1 Illustration of the pump color-controlled metadevice for coded terahertz switching. a Transmitted terahertz waves can be separately manipulated using two pumped lasers, each carrying different colors. The metadevice is a hybrid with arranged DBRs and a terahertz metasurface. **b** Schematic of a resonating system within one-unit cell supporting multiple coupled terahertz meta-atoms and two precisely aligned DBR mirrors. **c**, **d** Reflective optical micrographs of the fabricated metadevice with and without hybridizing visible metasurface, respectively. Scale bar: 25 μm. The golden section represents the gold metal metasurface, which has detailed geometrical properties as specified in the Supporting Information. The silicon island measures $15 \times 15\ \mu m^2$ and is represented by an orange square patch. **e**, **f** Reflectivity spectra for two DBRs corresponding to an area with CM_1 and for a location with CM_2. **g** Terahertz transmission spectrum of the color-coded metadevice

is simultaneously pumped by λ_1 and λ_2, both EIT resonances disappear (Fig. 2c). The experimental results found that two channels of EIT resonances can be independently tuned, suggesting a 2-bit pumping color-coded functionality. Note that the frequency of the resonance peak shifts during the modulation process due to the variation in charge accumulation on SRR capacitance-inductance resonance[53], as well as the near-field effect between coupling metaatoms. Turning now to discuss the encoding process in detail. To distinguish the coding state, we define the state without optical excitation as "0", which means no terahertz EIT modulation. And the fully modulated EIT with excitation is set as state "1". When only excited by λ_1, the first EIT resonance amplitude defined by peak 1 (P_1) and dip 1 (D_1) was effectively tuneable with various pump fluences as shown in Fig. 2e. Similarly, the second EIT resonance amplitude defined by peak 2 (P_2) and dip 2 (D_2) was eliminated for λ_2 excitation (Fig. 2f). It is evident that a greater pump fluence at 800 nm than at 400 nm is required to achieve maximum modulation. Namely, the pump efficiency of the two channels is different. The reason is that the absorption of 200-nm-thick Si film at different wavelengths varies, resulting in greater photoconductivity in silicon pumped by light at 400 nm than at 800 nm. Simultaneous excitation of two pump wavelengths will result in complete suppression of both EIT resonances (Fig. 2i). We can also alternatively keep one pumping wavelength in the excitation state while changing the pump fluences of the other pumping beam to perform encoding switching in different states (Fig. 2g, h). It should be noted that the crosstalk between the two encodings, indicating that λ_1 excitation can influence the second EIT resonance and λ_2 excitation can influence the first, which is most likely attributed to the residual impacts of DBR filtering and the coupling of near-field modes. On the one hand, the arranged DBRs

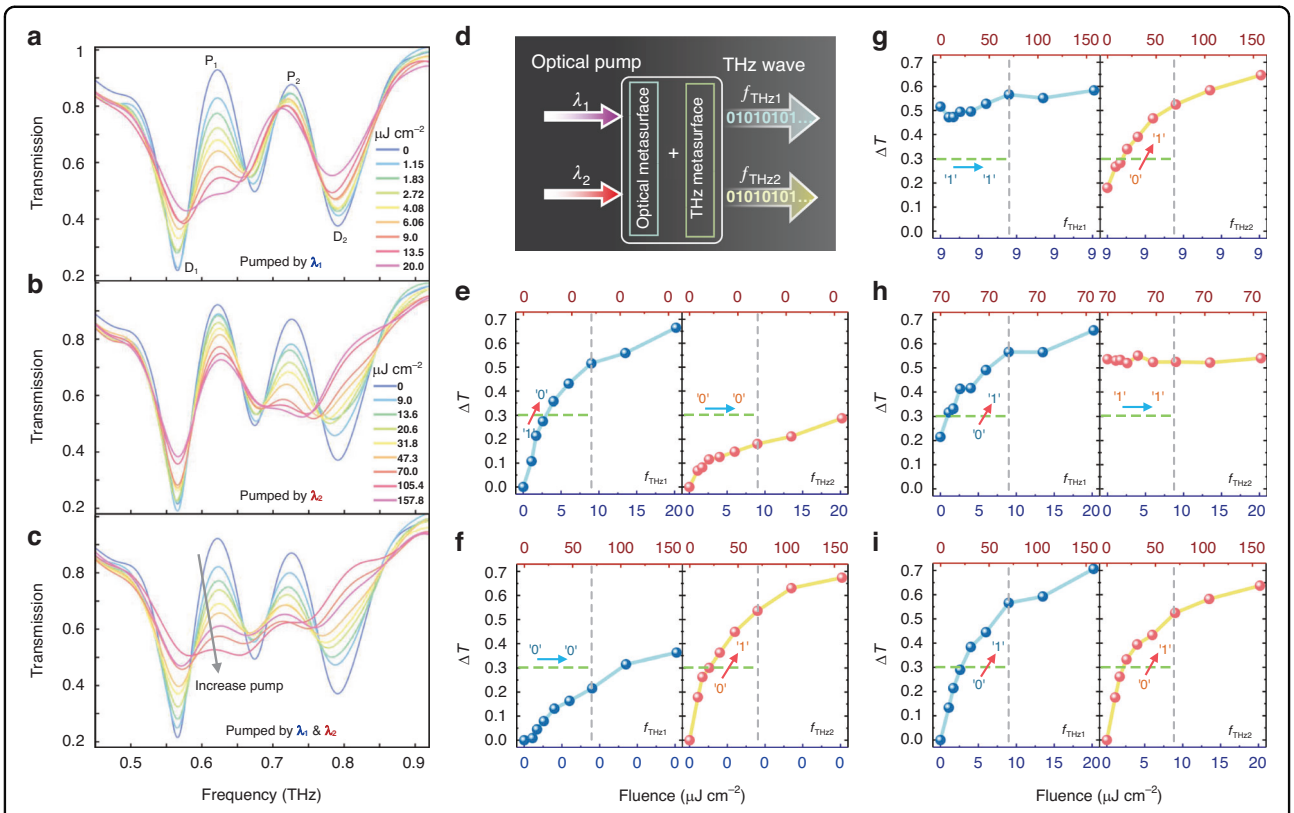

Fig. 2 Experimental results of 2-bit color metadevice to demonstrate its ability to control resonance modes by different pumping schemes coded by the wavelength. a–c THz transmission spectra of the metasurface array under various pump fluences with different coding configurations. **d** A flow diagram for realizing a programmable metasurface controlled by the optical pumping color. **e–i** Measured resonance transmission variations of CM_1 and CM_2 as a function of the pumping wavelength and fluence, respectively. The Green dashed line represents a transition threshold of two resonance states for different pumping conditions

are the primary cause of the problem. The grown DBRs cannot achieve a complete reflection of the corresponding wavelength (Fig. 1e, f), and the arranged DBRs also have a diffraction effect (Fig. S5) – a portion of the incident light is dispersed to other channels. On the other hand, the near-field coupling is partially responsible for the crosstalk, since the indirect interaction of two dark modes via a bright mode inside a subwavelength unit cell. The presence of crosstalk will result in the inability to independently encode each channel, which is certainly not what we want. Nevertheless, we can choose a suitable pump fluence (the gray dashed vertical lines) as the excitation to avoid crosstalk, meanwhile setting a threshold (the green dashed horizontal lines) for switching between "0" and "1" states. A 2-bit terahertz encoded modulation is possible when two separate light excitation channels are used, each with a different non-radiation loss of couple mode for independent control.

Ultrafast terahertz wave switching at 2-bit coding states

We demonstrated the ultrafast dynamic encoding modulation process extracted from time-resolve terahertz spectra with the exploitation of the nanosecond relaxation time of Si islands through femtosecond pulse pumping. The beginning point of light excitation is set at a pump-probe delay time of 0 ps when the photo-generation carrier of Si islands is stimulated. Subsequently, the excited carriers quickly restored to their initial state, along with an ultrafast modulation process of the color-coded metadevice. The transient dynamics of differential terahertz transmissions varying of Si film with the pump fluences under two pump laser wavelengths are shown in Fig. 3a, indicating that higher pump power can achieve greater modulation depth. However, this does not imply that the encoding modulation effect is improved by increasing the magnitude of pump fluence. We need to ensure that there is a clear distinction between "0" and "1", while simultaneously eliminating the crosstalk precisely caused by the pump interference as mentioned before. Therefore, the selection of an adequate pump fluence and switching threshold is taken into account. The threshold is chosen based on crosstalk in experimental testing to ensure that there is no interference between the two channels during the encoding process. Specifically, we must make sure that the green dashed lines in Fig. 2e–h do not cross the orange

and blue curves simultaneously. In the experiment, we select pump fluence of 9 $\mu J\ cm^{-2}$ at λ_1 and that of 70 $\mu J\ cm^{-2}$ at λ_2 as an excitation strategy for color encoding. The switching threshold between "0" and "1" states is set as 0.3 of differential EIT resonance amplitude (ΔT). Specifically, ΔT is less than 0.3 in the "0" state, while it is more than 0.3 in the "1" state. In this regard, we can claim that all-optical encoding for independently controlling the loss of CMs in binary channels with two stimulating wavelengths has been successfully achieved. The ultrafast modulation processes of differential EIT resonance amplitude within 1000 ps are measured by utilizing optical-pump terahertz-probe (OPTP) technology. By moving the relative time between the pump lights and the terahertz pulse arriving at the surface of the metadevice, the frequency-domain spectral as a function of time delay can be obtained. We show the ultrafast dynamic evolution of multiple encoding switches for various pump modulation approaches as illustrated by Fig. 3b–f. This behavior is based on the ultrafast terahertz switching of CM_1 and CM_2 resonances that are coded through two pumping wavelengths, respectively.

To better highlight the modulation changes brought out by the optical pump excitation, the transmission variation is defined as $T_v(\omega) = T_{without\ pump}(\omega) - T_{with\ pump}(\omega)$. Figure 4a depicts the EIT resonance transmission variations for the four coding states ("00", "01", "10", "11") in accordance with the standard of switching threshold. For the initial state of the metadevice at "00", the terahertz transmission spectrum, without pumping excitation, exhibits a dual-channel EIT resonance curve. The encoding process is 00-01/10-00 when each color (λ_1 *or* λ_2) is excited independently (Fig. 4b, c), while the red and blue parts mapped in Fig. 4 indicate the variations modulated by the pump, showing an ultrafast on-off-on photoswitching cycle within 1000 ps. When two color lights are excited simultaneously, the ultrafast encoding modulation is 00-11-00 (Fig. 4f). Also, alternatively activating one channel while modulating the other allows us to achieve an encoding process of 01/10-11-01/10 (Fig. 4d, e). Subsequently, we validated the transient dynamics of different coded states through the findings of numerical simulation. The variation of Si conductivity with time delay is first extracted from the experimentally measured transient differential terahertz transmission and fitted by bi-exponential functions (Fig. S2, Supporting Information), and then it is substituted into the finite element method simulation with COMSOL Multiphysics for numerical calculations. The entire ultrafast simulation can be regarded at different points in time as a quasi-steady state process since the relaxation time of silicon is far longer than a terahertz pulse's duration. The simulated terahertz transmission spectral variation at various pump-color-coded states described in Fig. S3 (Supporting Information) agrees well with the experimental results. Here we have implemented a light-control 2-bit ultrafast terahertz encoding operation, which has not been done before. In addition, the near-field distribution profiles of terahertz metasurface for different coded states are simulated in Fig. S4, Supporting Information. The discoveries that the localized electric field at the gap of the SRRs descends when the conductivity of the Si islands increases for the two couple modes provide insight into the microscopic mechanism of encoding. Besides, the changes in the electric field strength of one SRR mode affect that of the other SRR, hence influencing the resonance intensity of the two channels simultaneously. The distribution of the pump light field in DBRs also shows that optical beams with 800 nm and 400 nm excite difference channels, respectively (Fig. S5, Supporting Information). This reveals that the recombination of arranged DBRs and dual-EIT terahertz metasurface is the source of the 2-bit terahertz encoding's functionality, delivering a unique method for optically encoding terahertz information via terahertz metasurface in conjunction with optical metasurface.

Theoretical interpretation of 2-bit coding

The performance of 2-bit terahertz encoding originates from the modulation of non-radiative loss of two dark modes on SRRs, we can use the time-domain coupled mode theory (TCMT) to theoretically explain and fit the modulation of the spectral curves, which can be expressed as:

$$\frac{1}{2\pi}\frac{d\boldsymbol{a}}{dt} = (j\Omega - \Gamma)\boldsymbol{a} + D^T\boldsymbol{s}_+ \tag{1}$$

$$\boldsymbol{s}_- = C\boldsymbol{s}_+ + D\boldsymbol{a} \tag{2}$$

where $\boldsymbol{a}=(a_p, a_m, a_n)^T$ is the vector form of complex amplitudes of three resonance modes, $\boldsymbol{s}_+=(s_+^1, s_+^2)^T$ and $\boldsymbol{s}_-=(s_-^1, s_-^2)^T$ are the input and output amplitudes of each port, Ω is the matrix that describes the resonance frequencies and the near-field coupling coefficients, D is the coupling coefficients between resonances and input and output ports, Γ is the matrix of the dissipation rates and the indirect coupling coefficients. The terahertz metasurface can be modeled as a three-mode two-port system, we further define the matrices as[54]:

$$\Omega = \begin{pmatrix} f_p & \kappa_{pm} & \kappa_{pn} \\ \kappa_{pm} & f_m & \kappa_{mn} \\ \kappa_{pn} & \kappa_{mn} & f_n \end{pmatrix} \Gamma = \begin{pmatrix} \gamma_{p+}\gamma'_p & 0 & 0 \\ 0 & \gamma_{m+}\gamma'_m & \mathrm{X}_{mn} \\ 0 & \mathrm{X}_{mn} & \gamma_{n+}\gamma'_n \end{pmatrix} \tag{3}$$

$$C = \begin{pmatrix} r_{sub} & t_{sub} \\ t_{sub} & -r_{sub} \end{pmatrix} D = \begin{pmatrix} d_{1p} & d_{1m} & d_{1n} \\ d_{2p} & d_{2m} & d_{2n} \end{pmatrix} \tag{4}$$

where γ and γ' is the radiative and non-radiative loss, $r_{sub} = (1 - n_{sub})/(1 + n_{sub})$ and $t_{sub} = 2\sqrt{n_{sub}}/(1 + n_{sub})$

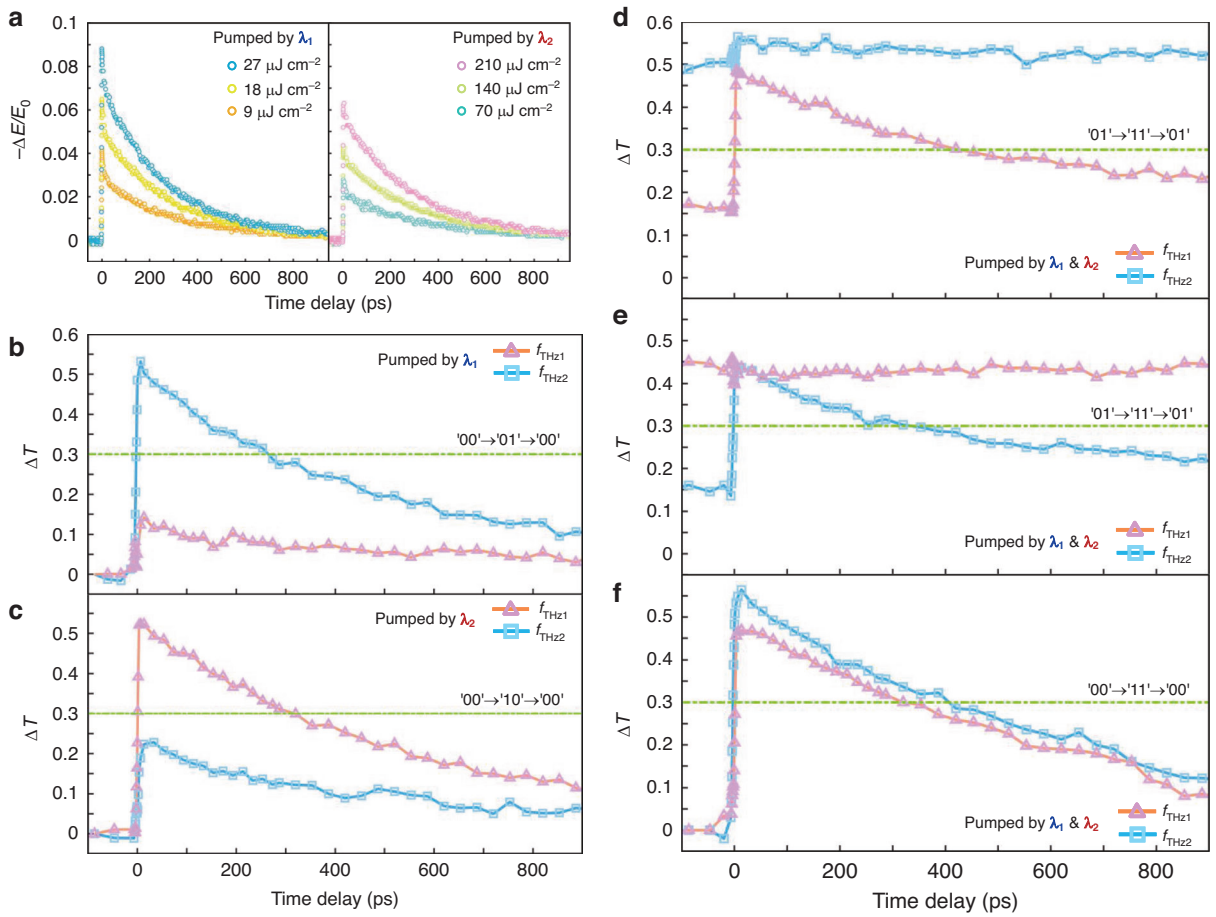

Fig. 3 Pumping color-coded ultrafast switching of THz bifunctionality. a Differential terahertz transmission revealed the fluence-dependent transient dynamics under two pump laser wavelengths. **b–f** Experimental demonstration of ultrafast THz switching of CM_1 and CM_2 resonances that are coded through two pumping wavelengths, respectively

denote the reflection and transmission of the bare substrate, respectively. Then we can obtain the expression of the transmission curve $t = s_-^2/s_+^1$ by calculating the coupled mode equation. X_{mn} is the far-field indirect coupling of modes a_m and a_n. Considering that the terahertz polarization direction follows the metal cut-wire, a_m and a_n are dark modes with no external coupling, therefore, $X_{mn} = 0$, $d_{1m} = d_{1n} = d_{2m} = d_{2n} = 0$. Ignoring the direct near-field coupling between two dark modes ($\kappa_{mn} = 0$), then the complex transmission coefficient can be obtained,

$$t = t_{sub} - \frac{2\sqrt{n_{sub}}\gamma_p}{1 + n_{sub}} \frac{W_m W_n + \kappa_{mn}}{W_p W_m W_n + W_m \kappa_{pn}^2 + W_n \kappa_{pm}^2} \tag{5}$$

where $W_j = -i(f - (f_j - i(\gamma_j + \gamma_j')))$ $(j = p, m, n)$.

Accordingly, we fitted the four encoding states examined in the experiment using the TCMT model (Fig. 5a), where the transparent solid lines indicate the fitting findings and the dotted lines represent the experimental data. Using numerical simulation, we first estimate the values of the coupling mode parameters and then make adjustments in line with the experimental results. We approach the transmission curves determined by the coupling mode theory to the experimental results using a genetic algorithm. Subsequently, the coupling mode parameters can be generated that are extremely near to the experimental curves. The detailed parameters for the four encoding states are listed in Table S3 in the Supporting Information. The TCMT model can accurately reproduce experimental results because it considers the interactions between various modes and the surrounding environment. Figure 5b–f illustrates how the extracted nonradiative damping rates of two dark modes (γ_m', γ_n') change during time delay under various pump excitations, which correspond to the ultrafast encoding switching of the simulated calculations and experimental observations, respectively. The transient behavior of other parameters can also be found in Supporting Information (Fig. S6).

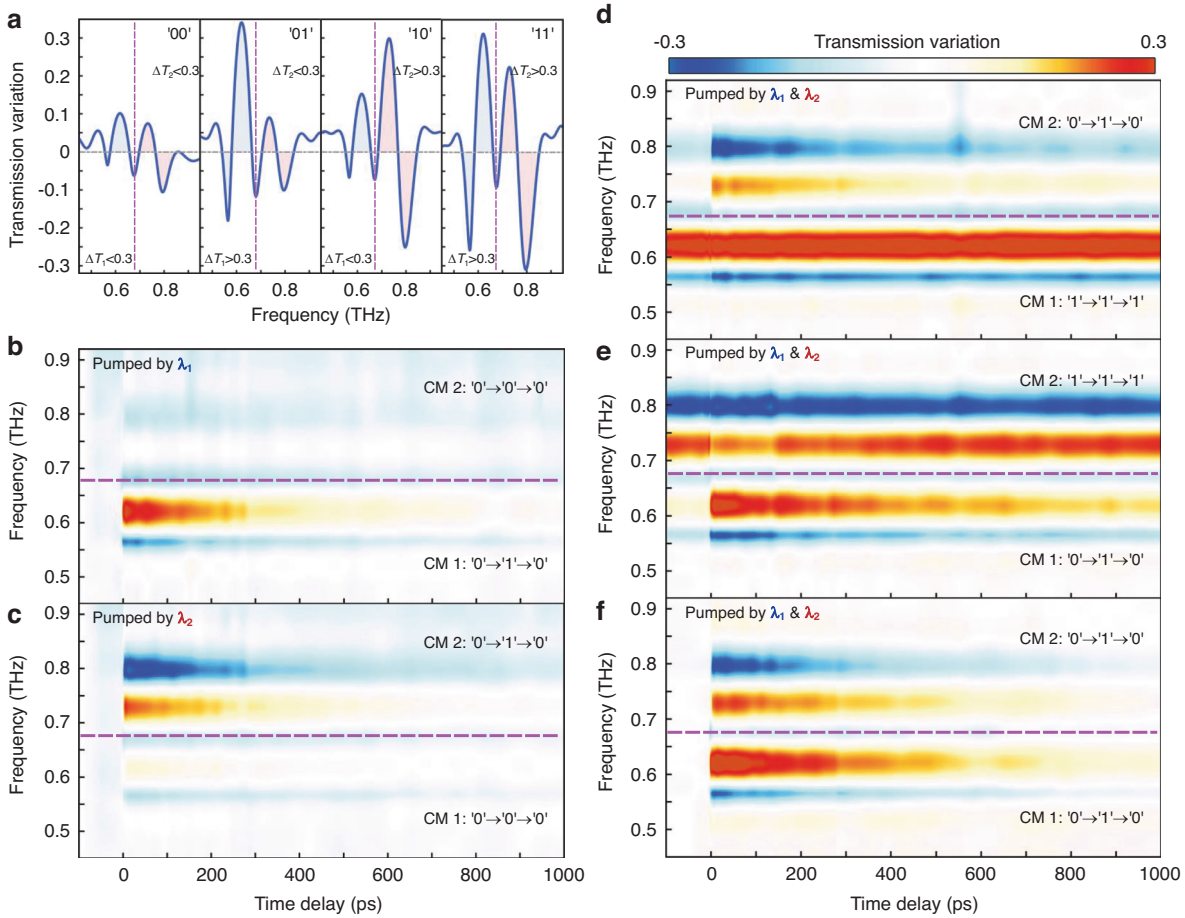

Fig. 4 Ultrafast THz response and spectral variation dynamics under different pumping configurations. a Measured THz transmission spectral variation at various coded states. **b**–**f** Pumping color driving THz spectral variation evolutions over the entire ultrafast on-off-on photoswitching cycle

The theoretical interpretation explains that transient non-radiative losses of CM_1 and CM_2 are the physical causes of the control of 2-bit ultrafast encoding. It is helpful to provide direction for the design of controllable lineshapes and corresponding function implementation.

Discussion

In summary, we proposed a novel method capable of all-optically controllable 2-bit terahertz encoding by combining photonic crystals and terahertz metasurface. The three-mode coupling supported by the terahertz metasurface allows for a dual-channel resonance spectrum and provides active loss-sensitive modulation. Additionally, the strategically placed DBRs create a particular spatial light distribution that filters respectively out the 400 nm and 800 nm pump wavelengths for color-pump terahertz switching. Through experimental testing, we were able to demonstrate the ultrafast behavior of encoding switching at the nanosecond scale, which excellently aligns with the intended effects of simulations. Moreover, the TCMT model provides a proper explanation for the encoding principle, which originates from the tailoring of non-radiative losses of the dissipative couple modes. Our strategy provides a new development way for optical coding terahertz modulation and further inspires the exploration of optical programming terahertz devices based on metasurfaces. This coding approach can be extended to multi-bit information processes and may be applied in the field of optical-controlled terahertz imaging.

Materials and methods

Sample fabrication

In the schematic of Fig. 1b, the terahertz metasurface is on a 1-mm-thick sapphire substrate and embedded with 200-nm-thick silicon islands. The second layer is on top of the z-cut quartz substrate and precisely adhered to the terahertz metasurface, making its DBRs filter the corresponding pumping wavelengths. The terahertz resonators are fabricated using two-step photolithography and metal

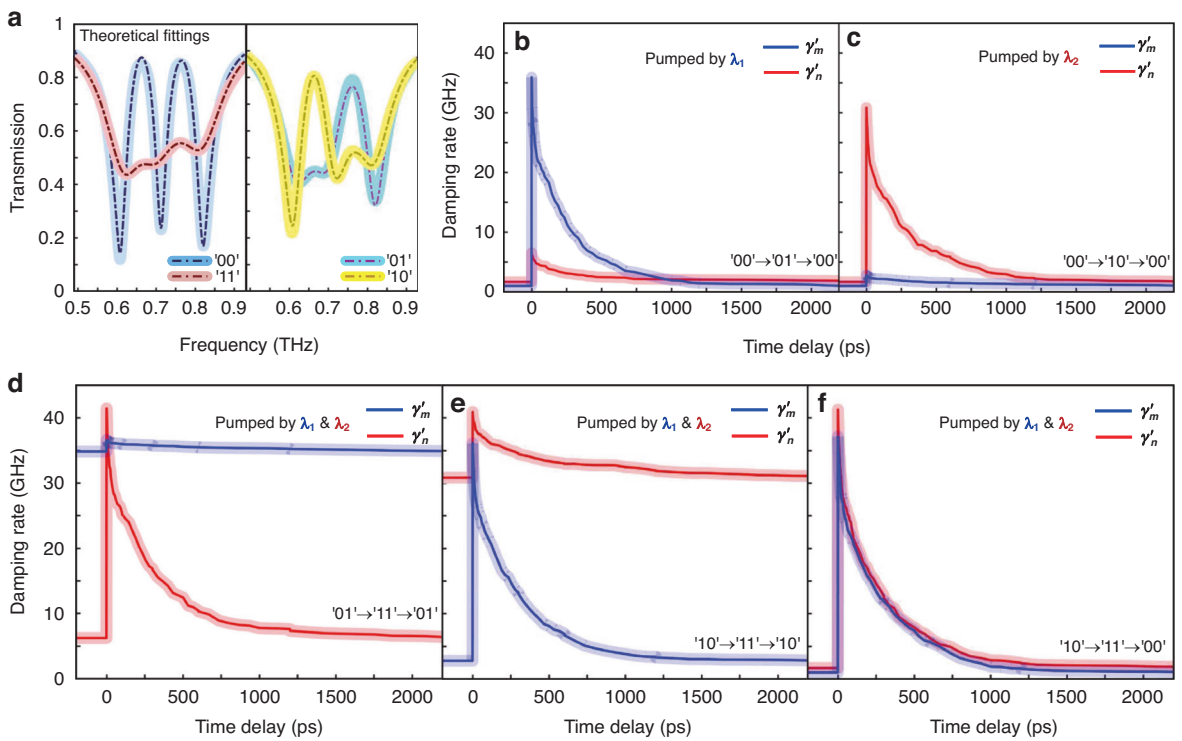

Fig. 5 Theoretical interpretation of temporal loss dynamics and physical elaboration of switching coded states. a TMCT fitted transmission spectra for different coded states. **b**–**f** Nonradiative damping rates of CM_1 and CM_2 that are tightly associated with pumping conditions as well as transient time delay

lift-off on a commercially available silicon-on-sapphire (SoS) substrate. Positive photoresist spin-coated on SoS is first patterned with silicon islands via a photomask, followed by lithography and development. The unprotected silicon is subsequently etched by reactive ion etching. The metallic array patterns precisely aligned with silicon islands are defined in the photoresists, followed by 200-nm-thick gold deposition and a lift-off process. The wavelength filtering sample consists of two kinds of DBRs, each with 8 periods of SiO_2 & Nb_2O_5 in the z-direction, that are separated by a 5-μm spacer in the y-direction. The DBRs are fabricated by magnetron sputtering coating equipment on a quartz substrate using an Nb_2O_5 composite target and Si composite target in O_2 gas with a substrate temperature of 200 °C. Unlike conventional DBR mirrors, our proposed DBRs are fabricated with an additional procedural photolithography technique to define the patterns of DBR_1 and DBR_2. For detailed structure parameters please see section 1 in the Supporting Information. An intuitive flowchart of sample fabrication processing is shown in Fig. S7.

Optical pump–terahertz probe spectroscopy

We use a home-built optical pump terahertz-probe spectroscopy setup to perform transmission measurements so that time-resolved terahertz spectra can be obtained. Femtosecond pulses generated from a Ti: Sapphire amplifier laser have a central wavelength of 800 nm, repetition rate of 1 kHz, and pulse width of ~100 fs. Linearly polarized terahertz waves are produced from a ZnTe crystal when illuminated by a femtosecond laser pulse train. The horizontal electric field of the transmitted terahertz wave is detected using a typical electro-optic sampling method in the time domain by a ZnTe crystal. To realize color-selective multifunctionality, the pumping beam is divided into two parts, one directly illuminating the metadevice and another one passing through a BBO crystal to generate a 400 nm femtosecond laser. The diameter of the pumping beam is ~5 mm which covers the terahertz spot uniformly on the sample. The whole setup is purged with dry gas to prevent the fingerprint water vapor absorption of terahertz waves. Far-field spectral amplitudes are derived from the measured data via numerical Fourier transformation and normalized with the reference signal of a pure substrate.

Electromagnetic simulation

Numerical simulations are executed using the finite element method (COMSOL Multiphysics®) to calculate the transmitted coefficients of the periodic terahertz resonators.

The periodic feature of meta-atoms is modeled using a unit cell with periodic boundary conditions in x- and y-directions, representing infinity in the xy plane. Two perfectly matched layers are selected in the z-direction to absorb the remaining energy after the field monitor. As for different coded states, the photoconductivity of silicon islands in CM_1 and CM_2 are independently controlled. In transient dynamic simulations, the time-dependent conductivity of silicon islands is substituted into the solver based on the formula $\Delta\sigma(t) = \varepsilon_0 c/d(n_a + n_s)[-\Delta E(t)/E_0]$. Here, $-\Delta E(t)/E_0$ is the fitted terahertz transmission amplitude variation by pumping a 200-nm-thick silicon film, n_a is the refractive index of air and n_s is the refractive index of the sapphire substrate. The c is the speed of light in a vacuum, d is the thickness of silicon film, and ε_0 is the vacuum permittivity constant. The conductivity of the gold is described using a Drude model with a plasma frequency ω_p=1.367 × 10^{16} rad s^{-1} and a collision frequency ω_c = 6.478 × 10^{13} rad s^{-1}. For the substrates, z-cut quartz and sapphire are modeled as a lossless dielectric with a permittivity of 3.9 and 9.6, respectively. The silicon islands without photoexcitation are set with a permittivity of 11.7.

Acknowledgements
The authors acknowledge financial support from the National Natural Science Foundation of China (62075240, 62305384), the National Key Research and Development Program of China (2020YFB2205800), and the Youth Innovation Talent Incubation Foundation of National University of Defense Technology (2023-lxy-fhij-007).

Author details
[1]College of Advanced Interdisciplinary Studies, National University of Defense Technology, Changsha, China. [2]Nanhu Laser Laboratory, National University of Defense Technology, Changsha, China. [3]Hunan Provincial Key Laboratory of High Energy Laser Technology, National University of Defense Technology, Changsha, China. [4]Institute for Quantum Science and Technology, College of Science, National University of Defense Technology, Changsha, China

Author contributions
W.H. and Y.H. conceived the idea. W.H., Z.R., and Y.H. designed the experiment and performed active measurements and all the simulations. S.H., Y.H., and S.W. fabricated the samples. W.H. and Z.Y. discussed and analyzed the measured data. T.J., X.C., and Y.H. supervised the theory and the measurements. W.H. prepared the manuscript with inputs from T.J. and Y.H.

Conflict of interest
The authors declare no competing interests.

Supplementary information The online version contains supplementary material available at https://doi.org/10.1038/s41377-024-01495-1.

Received: 21 November 2023 Revised: 1 May 2024 Accepted: 26 May 2024
Published online: 25 June 2024

References

1. Zhou, Z. et al. Prospects and applications of on-chip lasers. *eLight* **3**, 1 (2023).
2. Deng, W. et al. On-chip polarization- and frequency-division demultiplexing for multidimensional terahertz communication. *Laser Photon. Rev.* **16**, 2200136 (2022).
3. Jia, S. et al. Integrated dual-laser photonic chip for high-purity carrier generation enabling ultrafast terahertz wireless communications. *Nat. Commun.* **13**, 1388 (2022).
4. Chen, S. et al. Metasurface-empowered optical multiplexing and multifunction. *Adv. Mater.* **32**, 1805912 (2020).
5. Kumar, A. et al. Phototunable chip-scale topological photonics: 160 Gbps waveguide and demultiplexer for THz 6 G communication. *Nat. Commun.* **13**, 5404 (2022).
6. Yang, J. et al. Active optical metasurfaces: comprehensive review on physics, mechanisms, and prospective applications. *Rep. Prog. Phys.* **85**, 036101 (2022).
7. Huang, L. et al. Resonant leaky modes in all-dielectric metasystems: fundamentals and applications. *Phys. Rep.* **1008**, 1–66 (2023).
8. Kim, J. et al. Tunable metasurfaces towards versatile metalenses and metaholograms: a review. *Adv. Photon.* **4**, 024001 (2022).
9. Feng, Z. et al. Dual-band polarized upconversion photoluminescence enhanced by resonant dielectric metasurfaces. *eLight* **3**, 21 (2023).
10. Li, L. et al. Intelligent metasurfaces: control, communication and computing. *eLight* **2**, 7 (2022).
11. Ma, Q. et al. Directly wireless communication of human minds via non-invasive brain-computer-metasurface platform. *eLight* **2**, 11 (2022).
12. Zhu, Y. et al. Metasurfaces designed by a bidirectional deep neural network and iterative algorithm for generating quantitative field distributions. *Light: Adv. Manuf.* **4**, 9 (2023).
13. Lan, F. et al. Real-time programmable metasurface for terahertz multifunctional wave front engineering. *Light Sci. Appl.* **12**, 191 (2023).
14. Chen, B. et al. Electrically addressable integrated intelligent terahertz metasurface. *Sci. Adv.* **8**, eadd1296, (2022).
15. Zhang, L. et al. Highly tunable cascaded metasurfaces for continuous two-dimensional beam steering. *Adv. Sci.* 10, e2300542 (2023).
16. Zhang, J. C. et al. A 6G meta-device for 3D varifocal. *Sci. Adv.* **9**, eadf8478 (2023).
17. Degl'Innocenti, R. et al. Recent progress in terahertz metamaterial modulators. *Nanophotonics* **11**, 1485–1514 (2022).
18. Zang, X. et al. Metasurfaces for manipulating terahertz waves. *Light Adv. Manuf.* **2**, 10 (2021).
19. Petrov, N. V. et al. Design of broadband terahertz vector and vortex beams: I. Review of materials and components. *Light: Adv. Manuf.* **3**, 640-652 (2022).
20. Zhao, H. J. et al. Active terahertz beam manipulation with photonic spin conversion based on a liquid crystal Pancharatnam–Berry metadevice. *Photon. Res.* **10**, 2658 (2022).
21. Fu, X. et al. Flexible terahertz beam manipulations based on liquid-crystal-integrated programmable metasurfaces. *ACS Appl. Mater. Interfaces* **14**, 22287–22294 (2022).
22. Yu, H. et al. Photo-reconfigurable and electrically switchable spatial terahertz wave modulator. *Chin. Opt. Express* **21**, 010002 (2023).
23. Chen, B. et al. Directional terahertz holography with thermally active Janus metasurface. *Light Sci. Appl.* **12**, 136 (2023).
24. Chen, X. et al. Reconfigurable and nonvolatile terahertz metadevices based on a phase-change material. *ACS Photon.* **9**, 1638–1646 (2022).
25. Pitchappa, P. et al. Volatile ultrafast switching at multilevel nonvolatile states of phase change material for active flexible terahertz metadevices. *Adv. Funct. Mater.* **31**, 2100200 (2021).
26. Zhuang, X. et al. Active terahertz beam steering based on mechanical deformation of liquid crystal elastomer metasurface. *Light Sci. Appl.* **12**, 14 (2023).
27. Chen, C. et al. On-demand terahertz surface wave generation with microelectromechanical-system-based metasurface. *Optica* **9**, 17–25 (2022).
28. Huang, J. et al. BICs-enhanced active terahertz wavefront modulator enabled by laser-cut graphene ribbons. *Photon. Res.* **11**, 1185 (2023).
29. Li, Q. et al. Gate-tuned graphene meta-devices for dynamically controlling terahertz wavefronts. *Nanophotonics* **11**, 2085–2096 (2022).
30. Cong, L. et al. All-optical active THz metasurfaces for ultrafast polarization switching and dynamic beam splitting. *Light Sci. Appl.* **7**, 28 (2018).
31. Manjappa, M. et al. Solution-processed lead iodide for ultrafast all-optical switching of terahertz photonic devices. *Adv. Mater.* **31**, e1901455 (2019).
32. Cong, L. et al. Spatiotemporal dielectric metasurfaces for unidirectional propagation and reconfigurable steering of terahertz beams. *Adv. Mater.* **32**, e2001418 (2020).
33. Kumar, A. et al. Excitons in 2D perovskites for ultrafast terahertz photonic devices. *Sci. Adv.* **6**, eaax8821, (2020).

34. He, W. et al. Ultrafast all-optical terahertz modulation based on an inverse-designed metasurface. *Photon. Res.* **9**, 1099–1108 (2021).
35. Jiao, Y. et al. Photoactive terahertz metasurfaces for ultrafast switchable sensing of colorectal cells. *Mater. Horiz.* **9**, 2984–2992 (2022).
36. Cong, L. et al. Temporal loss boundary engineered photonic cavity. *Nat. Commun.* **12**, 6940 (2021).
37. Zhou, H. et al. Optically controlled dielectric metasurfaces for dynamic dual-mode modulation on terahertz waves. *Adv. Photon.* **5**, 026005 (2023).
38. Lou, J. et al. Calibration-free, high-precision, and robust terahertz ultrafast metasurfaces for monitoring gastric cancers. *Proc. Natl Acad. Sci. USA* **119**, e2209218119 (2022).
39. Sun, H. et al. Ultrafast all-optical switching of dual-band plasmon-induced transparency in terahertz metamaterials. *Chin. Opt. Lett.* **20**, 013701 (2022).
40. Lim, W. X. et al. Ultrafast all-optical switching of germanium-based flexible metaphotonic devices. *Adv. Mater.* **30**, 1705331 (2018).
41. Sun, H. et al. Ultrafast polarization-dependent all-optical switching of germanium-based metaphotonic devices. *Photon.Res.* **8**, 263–270 (2020).
42. Degert, J. et al. Ultrafast, broadband and tunable terahertz reflector and neutral density filter based on high resistivity silicon. *Opt. Express* **30**, 18995–19004 (2022).
43. Hu, Y. et al. Spatiotemporal lineshape tailoring in BIC-mediated reconfigurable metamaterials. *Adv. Funct. Mater.* **32**, 2270194 (2022).
44. Hu, S. et al. Dual-dimensional EIT manipulation for angle-multiplexed ultrafast terahertz switching. *ACS Photon.* **10**, 2182–2191 (2023).
45. Hu, Y. et al. Bifunctional spatiotemporal metasurfaces for incident angle-tunable and ultrafast optically switchable electromagnetically induced transparency. *Small* **17**, 2006489 (2021).
46. Stantchev, R. I. et al. Compressed sensing with near-field THz radiation. *Optica* **4**, 989–992 (2017).
47. Stantchev, R. I. et al. Noninvasive, near-field terahertz imaging of hidden objects using a single-pixel detector. *Sci. Adv.* **2**, e1600190 (2016).
48. Chen, S.-C. et al. Terahertz wave near-field compressive imaging with a spatial resolution of over λ/100. *Opt. Lett.* **44**, 21–24 (2019).
49. Shang, Y. et al. Terahertz image reconstruction based on compressed sensing and inverse Fresnel diffraction. *Opt. Express* **27**, 14725–14735 (2019).
50. Stantchev, R. I. et al. Real-time terahertz imaging with a single-pixel detector. *Nat. Commun.* **11**, 2535 (2020).
51. Srivastava, Y. K. et al. MoS2 for ultrafast all-optical switching and modulation of THz fano metaphotonic devices. *Adv. Opt. Mater.* **5**, 1700762 (2017).
52. Hu, Y. et al. Ultrafast terahertz transmission/group delay switching in photoactive WSe2-functionalized metaphotonic devices. *Nano Energy* **68**, 104280 (2020).
53. Chen, H. T. et al. Experimental demonstration of frequency-agile terahertz metamaterials. *Nat. Photon.* **2**, 295–298 (2008).
54. Huang, W. et al. A complete phase diagram for dark-bright coupled plasmonic systems: applicability of Fano's formula. *Nanophotonics* **9**, 3251–3262 (2020).